Picosecond-Scale Ultrafast Many-Body Dynamics in an Ultracold Rydberg-Excited Atomic Mott Insulator

V. Bharti[1,*] S. Sugawa[1,2,*,‡,§] M. Mizoguchi,[1,*] M. Kunimi[1,†] Y. Zhang,[1,3] S. de Léséleuc[1,2]
T. Tomita[1] T. Franz,[4] M. Weidemüller[4] and K. Ohmori[1,2,‖]

[1]*Institute for Molecular Science, National Institutes of Natural Sciences, Okazaki 444-8585, Japan*
[2]*SOKENDAI (The Graduate University for Advanced Studies), Okazaki 444-8585, Japan*
[3]*College of Physics and Electronic Engineering, and Collaborative Innovation Center of Extreme Optics,
Shanxi University, Taiyuan, Shanxi 030006, China*
[4]*Physikalisches Institut, Universität Heidelberg, Im Neuenheimer Feld 226, 69120 Heidelberg, Germany*

We report the observation and control of ultrafast many-body dynamics of electrons in ultracold Rydberg-excited atoms, spatially ordered in a three-dimensional Mott insulator (MI) with unity filling in an optical lattice. By mapping out the time-domain Ramsey interferometry in the picosecond timescale, we can deduce entanglement growth indicating the emergence of many-body correlations via dipolar forces. We analyze our observations with different theoretical approaches and find that the semiclassical model breaks down, thus indicating that quantum fluctuations play a decisive role in the observed dynamics. Combining picosecond Rydberg excitation with MI lattice thus provides a platform for simulating nonequilibrium dynamics of strongly correlated systems in synthetic ultracold atomic crystals, such as in a metal-like quantum gas regime.

Well-controlled isolated quantum systems have become essential experimental platforms for addressing quantum many-body problems that are inaccessible with classical computers [1]. Of particular interest is the understanding of the emergence of many-body correlations and entanglement that arise from long-range interactions among particles. Quantum spin models with long-range interactions have been realized in various settings including trapped ions [2–4], polar molecules [5,6], and magnetic atoms [7,8]. Because of their exquisite controllability and, in particular, tunable long-range interactions, Rydberg gases have recently emerged as promising systems for studying many-body problems [9–12]. Spin models have been implemented in one, two, or three dimensions with spatially ordered and disordered atomic ensembles [13–25]. With these systems, fundamental questions of many-body spin physics can be addressed, such as the origin of quantum magnetism and the role of many-body correlations and entanglement during nonequilibrium dynamics.

While many experimental studies on many-body dynamics have employed continuous-wave (cw) lasers to excite atoms to Rydberg states, broadband pulsed lasers are expected to offer unique possibilities for exploring novel dynamical features of strongly-correlated electrons. With cw lasers, the simultaneous excitation of atomic pairs at a short distance, typically below several microns, is inhibited due to the Rydberg blockade effect [26–30]. Facilitated excitation with frequency-detuned cw lasers allows one to reach shorter distances [31–35]. Alternatively, broadband

pulsed laser excitation with an ultrashort pulse can directly circumvent the blockade effect even down to nearest-neighbor (NN) distances in optical lattices [36]. This leads to high Rydberg densities yielding GHz-scale interactions, which are orders of magnitude larger than that of the cw approach [13,23,24]. Such interaction timescales are orders of magnitude shorter than the lifetimes of the Rydberg states (including effects of blackbody radiation) and typical timescales set by environmental noise, thermal motion, and laser phase noise [37–39], thus rendering it possible to explore long-time nonequilibrium dynamics.

In a previous study, using a spatially disordered ensemble of rubidium (Rb) atoms at microkelvin temperatures in an optical dipole trap, we revealed the ultrafast many-body dynamics of electronic coherences between the ground and high-lying electronic (Rydberg) states [13]. Tens of particles were shown to get correlated within several hundreds of picoseconds. In this Letter, we report the observation of ultrafast nonequilibrium many-body dynamics of highly excited electrons, created from atoms in a three-dimensional Mott insulator (MI) with unity filling. We analyze the observed time-domain Ramsey dynamics with theoretical models of increasing complexity providing insights into the role of long-range quantum correlations for the nonequilibrium dynamics.

Experimental setup.—Our experimental system is schematically shown in Fig. 1(a). A number $N \approx 3 \times 10^4$ of ^{87}Rb atoms is trapped in a three-dimensional optical lattice at a lattice depth of $\sim 20 E_R$, forming a unity-filling
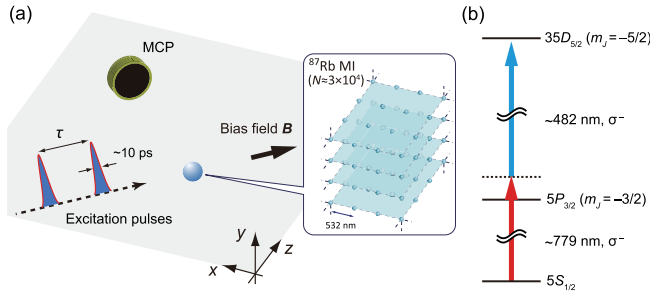
FIG. 1.   (a) Experimental schematic. The atoms are irradiated with a pair of picosecond excitation pulses with tunable time-delay τ, during which the system evolves. The atoms in the Rydberg state are detected as ions with a MCP following the field ionization. (b) The atoms in the ground state are coherently excited to the $35D$ state by a two-photon laser excitation with circularly polarized blue and IR laser pulses propagating along the bias magnetic field direction.

MI [36,40]. Here, $E_R = h^2/2m_{Rb}\lambda^2$ is the recoil energy of the lattice laser operating at $\lambda = 1064$ nm, and m_{Rb} is the ^{87}Rb mass. The optical lattice is formed by superimposing three orthogonal standing waves of light, thereby creating a trap potential in a cubic lattice geometry with a lattice constant of $a_{lat} = 532$ nm. The Rb atoms in the MI act as a nearly defect-free three-dimensional array of single atoms.

The atoms in the hyperfine ground state $5S_{1/2}$, $|F = 2$, $m_F = -2\rangle$ are coupled to a Rydberg state via a two-photon optical transition using broadband picosecond laser pulses with their wavelengths tuned to ~779 (IR) and ~482 nm (blue) [see Fig. 1(b)] [40]. The IR and blue laser pulses are irradiated simultaneously to the atoms and the polarizations of the laser pulses are both set to σ^- so that only $|\nu D_{5/2}$, $m_J = -5/2\rangle$ can be populated, following the optical selection rules. In the present study, the principal quantum number $\nu = 35$ is chosen, and the center frequencies are tuned to the corresponding two-photon resonance [40].

Ramsey interferogram.—We measure the electron dynamics by time-domain Ramsey interferometry with a pair of excitation laser pulses [40,50–52]. The pump pulse creates a superposition of the $5S_{1/2}$ and $35D_{5/2}$ states. The system then undergoes many-body dynamics that originates from anisotropic long-range interactions among Rydberg atoms until the probe pulse is irradiated on the atoms. The time-delay between the pump and probe pulses is tuned using an optical delay line interferometer [52]. The pump and probe pulses have identical energies as well as spatial and temporal profiles of their electric fields.

Ramsey oscillations are observed by measuring the final Rydberg population as a function of the time-delay τ. After irradiating the probe pulse, we apply a pulsed electric field to ionize the Rydberg atoms, which are finally detected with a microchannel plate (MCP) as ions [40]. Figures 2(a) and 2(b) show the Ramsey interferograms at $\tau \sim 50$
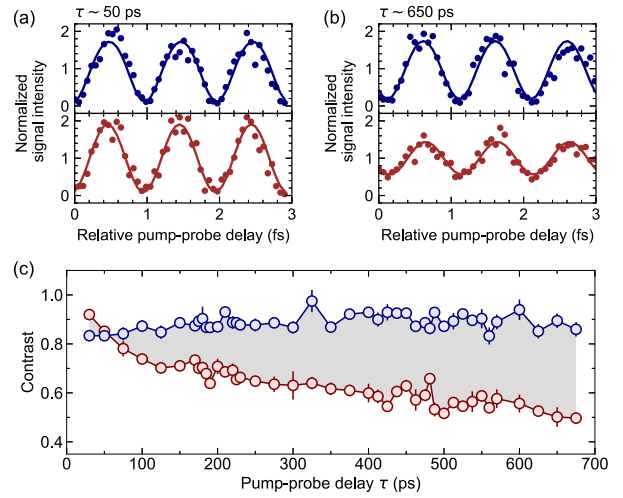

FIG. 2.   (a),(b) Time-domain Ramsey interferograms for the MI (red) and reference clouds (blue) for two different delays [$\tau \sim 50$ ps (a) and $\tau \sim 650$ ps (b)]. The solid lines are theoretical fits to the data. Each interferogram is rescaled using the offset value of the sinusoidal function that best fits the data. (c) The contrasts of the Ramsey signals for the MI (red) and the reference clouds (blue) obtained with the Rydberg state population $p_e = 5.6(2)\%$. Error bars represent the standard error of the mean.

and ~650 ps, respectively, exhibiting oscillations at a period of ~1 femtosecond (fs) corresponding to the frequency of the $5S_{1/2} - 35D_{5/2}$ two-photon transition ($E_{eg}/\hbar \sim 2\pi \times 10^{15}$ Hz). The relative time delay in each Ramsey interferogram is calibrated with attosecond precision using an optical interference signal from a He-Ne laser while we scan the time delay.

To evaluate the effect arising from atomic interaction, we use the remaining atoms to record Ramsey oscillations of a reference "low-density" cloud with a mean atomic distance $n^{-1/3} \sim 3.5$ μm in each experimental sequence. The low-density clouds are prepared by expanding and transferring the atoms to a deep cigar-shaped optical dipole trap with a depth of tens of microkelvin after the first Ramsey sequence for the MI atoms [40].

Each Ramsey interferogram is characterized by the contrast $C(\geq 0)$ and the phase $\phi \in [-\pi, \pi)$, which are obtained by fitting the interferograms with a function of the form $\propto 1 + C\cos(E_{eg}\tau/\hbar + \phi)$. For the reference measurement, a systematic change in the remaining atom number is taken into account by introducing a correction factor to the above fitting function [40].

The contrasts of the Ramsey oscillations for the MI and the reference clouds are depicted in Fig. 2(c). The contrasts for the reference clouds are constant over the entire delay range, which indicates that single-atom decoherence mechanisms can safely be neglected. On the contrary, the contrasts for the MI clouds decrease as the time-delay increases, which will be analyzed in more detail below. In the following analysis, we
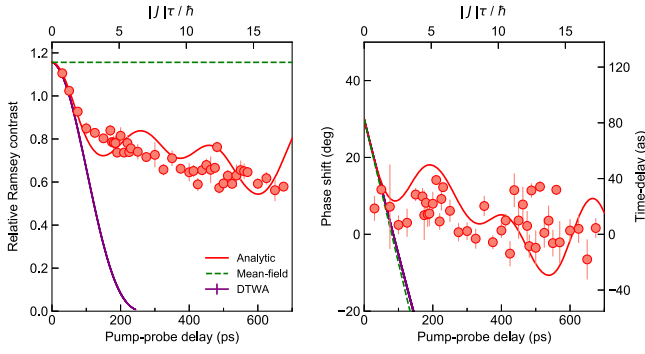
FIG. 3. Experimental relative Ramsey contrasts and phase shifts (red circles) compared with different theoretical approaches. The relative Ramsey contrasts and phase shifts at $\tau = 0$ in the theories are adjusted to values identical to those obtained with the analysis with the analytical solution. The error bars represent the standard error of the mean.

introduce the relative Ramsey contrast $\mathcal{C}_R = C_H/C_L$ and the phase shift $\phi_R = \phi_H - \phi_L \in [-\pi, \pi)$, which are summarized in Fig. 3. Here, the subscript H (L) represents "high-density" MI clouds (low-density reference clouds).

The model Hamiltonian.—We analyze our observation with the quantum Ising model [53–58]. The model Hamiltonian is

$$\hat{H} = \sum_j \frac{1}{2} E_{eg} \hat{\sigma}_j^z + \sum_{j<k} U_{jk} \hat{n}_j \hat{n}_k, \qquad (1)$$

where the Rydberg state ($|e\rangle$) and the ground state ($|g\rangle$) are mapped to the pseudospin states. Here $\hat{n}_j = |e\rangle\langle e|_j = (1 + \hat{\sigma}_j^z)/2$, $\hat{\sigma}_j^{x,y,z}$ are the Pauli operators for the jth atom, and U_{jk} is the long-range anisotropic interaction between the jth and kth Rydberg atoms. The second term in the Hamiltonian describes the effective interactions among spin-1/2 particles, which create correlations and entanglement among distant atoms. We considered an effective van der Waals (vdW) potential of the form $U_{jk} = -C_6(1 - 3\cos^2\theta_{jk})^2/r_{jk}^6$, where C_6 is the vdW coefficient and r_{jk} is the distance between the jth and kth atoms, and θ_{jk} is the angle between the quantization axis and a vector from the jth to the kth atom [40]. Because of the complexity of predicting the actual pair potential caused by an increasing number of contributing pair states as well as higher-order couplings beyond the dipolar interactions [59], the C_6 value serves as a free fitting parameter being determined by the model below.

Exact analytical solution.—The Ising spin model in Eq. (1) has an exact analytical solution that fully takes into account many-body correlations [53–58]. The Ramsey signal of the jth atom is

$$P_{e,j}(\tau) = 2p_e p_g \text{Re}\{1 + G_j(\tau)\exp[i(E_{eg}\tau/\hbar + \varphi_j)]\}, \quad (2)$$

where p_e (p_g) is the Rydberg (ground) state population after the pump excitation, $G_j(\tau) = \Pi_{k\neq j}^N p_g + p_e \exp(iU_{jk}\tau/\hbar)$, and φ_j is the phase acquired during the pulse excitation due to the ac-Stark shift [13]. The single-particle function $G_j(\tau)$ contains information about the many-body effect encoded in the Ramsey signal and is related to the Larmor precession of the jth pseudo-spin via $\langle\hat{\sigma}_j^+(\tau)\rangle = G_j(\tau)e^{iE_{eg}\tau/\hbar}\langle\hat{\sigma}_j^+(0)\rangle$, where $\hat{\sigma}_j^+ = \hat{\sigma}_j^x + i\hat{\sigma}_j^y$. The Ramsey contrast of the jth atom $\mathcal{C}_{R,j}(\tau)$ is determined by $|G_j(\tau)|$, its relative phase shift $\phi_{R,j}(\tau)$ by $\arg[G_j(\tau)]$. The total signal is obtained by taking the average of the ensemble, $\bar{P}_e(\tau) = (1/N)\sum_{j=1}^N P_{e,j}(\tau)$. The pump pulse creates a superposition of many-particle quantum states representing a different number and arrangement of the Rydberg atoms on the lattice. During the time delay, each many-particle state acquires a phase according to the long-range interactions and interferes coherently to eventually give rise to the strongly correlated many-body quantum state.

Comparing the experimental results to the analytical solution allows us to benchmark our quantum simulator. We determine the C_6 value by fitting the above exact analytical solution to the Ramsey contrasts. Using the C_6 value as the only free parameter, we obtain good agreement with the experimental contrast data for $C_6/\hbar = 371(6)$ MHz μm^6 as shown by the red curve in Fig. 3, except for small temporal undulations in the theory. Here, we forced the theoretical curve to pass through the data point at the shortest time delay near $\tau = 0$. The angle-averaged vdW coefficient obtained from the fitted C_6 value agrees within a factor of 3 with a numerical estimate valid at a large atomic distance [59]. Since our system is large, nearly defect-free, and thus essentially homogeneous, the dynamics is approximated well near the thermodynamic limit of $N \to \infty$, where the finite-size effect is neglected [40]. The C_6 value extracted from the contrast decay can also consistently account for the slow decreasing trend in the phase shift as shown in Fig. 3, where the phase shift at $\tau = 0$ was used as a free fitting parameter [40]. The nonzero phase shift at $\tau = 0$ could possibly arise from the difference in the ac-Stark shifts between the two clouds [60]. To gain further insights into the role of quantum correlations, we compared our result with two models of increasing complexity.

Mean-field theory.—First, we analyze the observations in the mean-field approximation. The interaction energy shift of one Rydberg atom is given by the sum of the interactions with the surrounding $N - 1$ atoms, $U_{MF,j} = \sum_{k=1,k\neq j}^N p_e U_{jk}$. The mean-field approximation predicts that a relative Ramsey contrast $\mathcal{C}_R(\tau) = 1$, independent of C_6 and τ, and a phase shift $\phi_R(\tau) = U_{MF,j}\tau/\hbar$, evolving linearly with τ. The green dashed lines in Fig. 3 show the prediction for the relative Ramsey contrast and phase shift using the C_6 determined as described above.

The obvious failure of the mean-field prediction is more pronounced in our ordered and nearly defect-free atomic array with a larger number of atoms than in disordered ensembles, including atoms in an optical lattice with defects (i.e., nonunity filling) and small arrays [6]. Inhomogeneity in the mean-field energy shift leads to decay and nonlinear time evolution in the ensemble-averaged contrast and phase shift, respectively.

Semiclassical theory.—The discrete truncated Wigner approximation (DTWA) is a semiclassical approach, in which the quantum uncertainty in the spin state is incorporated by the initial sampling with the discrete Wigner function [61,62]. The DTWA has successfully captured quantum spin dynamics in various studies [7,8,20,21]. The comparison between our experimental result and the DTWA simulation performed with a $31^3 (\sim 3 \times 10^4)$-site cubic array is shown in the purple solid curves in Fig. 3. The agreement can be confirmed only up to $\tau \sim 2\hbar/|J|$, where $J \sim -1.6 C_6/a_{\text{lat}}^6$ is the strongest NN interaction strength. The DTWA includes initial quantum fluctuations of the spin state so that quantum corrections up to their leading order can be included in an effective mean-field approximation. Accordingly, the timescale on which the DTWA is quantitatively valid is generally set by $\mathcal{O}(\hbar/|J|)$ [63,64], where the initial quantum fluctuations still dominate the dynamics. For $p_e \sim 50\%$, as in previous experiments on many-body spin dynamics [20,21], DTWA accidentally coincides with the exact solution [61]. In our setting, however, DTWA fails for a longer time delay τ as the population p_e is much smaller than 50%.

Entanglement buildup.—Our Ramsey interferometry can directly measure the evolution of the entanglement [40]. During the many-body dynamics, the initial many-particle state evolved into a highly entangled state and consequently each single-particle reduced state $\hat{\rho}$ decreases its local purity. The nth Rényi entanglement entropy $S^{(n)}(\tau) = -\log_2[\text{Tr}(\hat{\rho}^n)]$ of the single-particle subsystem is a suitable measure to characterize its evolution. By definition, the Rényi entropy is zero for the product states and takes positive values for the entangled states. Figure 4 shows the 2nd order Rényi entropies obtained by extracting $\hat{\rho}(\tau)$ from the data in Fig. 3, assuming the thermodynamic limit of $N \to \infty$. Consistent with the theoretical calculation, we observe ultrafast growth of the single-site entanglement entropy toward the theoretical upper limit, which corresponds to the case of $\mathcal{C}_R = 0$. The errors due to the finite size of the array are small and estimated to be less than 5%. The timescale of the entanglement growth being $|J|\tau/\hbar \gg 1$ indicates that long-range interactions beyond the 1st NNs are involved in the dynamics, which is also consistent with our cluster expansion analysis [40].

In conclusion, we developed a platform for simulating many-body dynamics on the picosecond-scale, by utilizing our ultrafast technique and an atomic Mott insulator as a
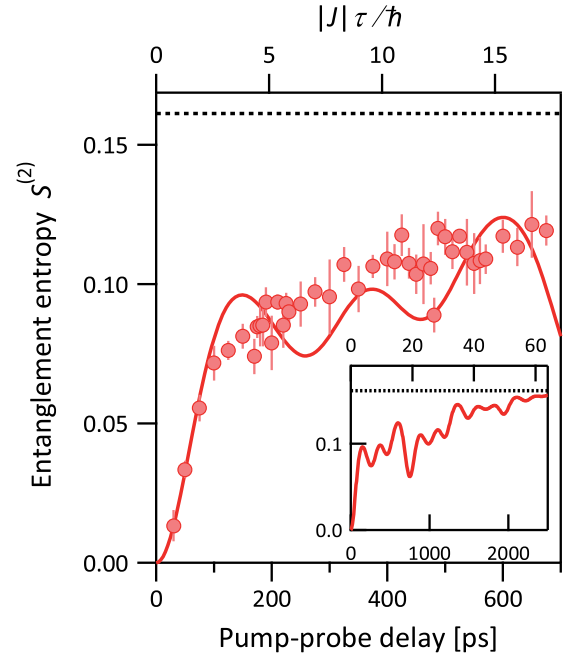

FIG. 4. Ultrafast growth of single-site entanglement entropy. The measured 2nd order Rényi entropies (circles) are shown with the theoretical calculation based on the exact solution assuming $N \to \infty$ (solid curve). The dashed line is the theoretical upper limit set by the population p_e.

large-scale array. By comparing our observation with the solution with full many-body correlations as well as those of the mean-field and semiclassical theories, we identified the emergence of long-range many-body correlations in our ultrafast dynamics. Noteworthy, our unambiguous experimental identification of the essential role of many-body correlations is strongly supported by the measurability not only of the contrast decay in the Ramsey signal but also of its minute phase shift on the attosecond timescale. Furthermore, we measured the time evolution of the single-site entanglement entropy on the picosecond timescale.

The remaining quantitative difference between the experiment and the many-body simulation could arise from the approximation of describing the Rydberg pair potential as a single effective potential as well as neglecting the finite width of the quantum ground-state atomic wave function at each lattice site [65–67]. The latter could lead to uncertainty in the interaction energies between atoms. These two factors, which are beyond the scope of our analysis, could smear out the small temporal undulations in the many-body theories.

Our work can be directly extended to other interaction regimes by tuning the principal quantum number and the orbital angular momentum. Other quantum spin models such as the Heisenberg model [20,68] and the *XY* model [21] could be implemented by employing direct broadband laser excitation to two Rydberg states. Our ultrafast approach can be combined with a microscope

[14,15,17,22] as well as an optical tweezer array [10–12,16,19,23,24,65] to reveal ultrafast dynamics with single-site resolution. The long-time dynamics, orders of magnitude longer than the interaction timescale, could address many-body thermalization and localization problems [69–71] without effects from environmental noise and the radiative lifetime. A measurement of the collective spin fluctuations using our Ramsey scheme can identify the correlation buildup [72]. Most interestingly, our ultrafast Ramsey measurement could uncover the many-body electronic states and the nonequilibrium dynamics in a metal-like quantum gas regime, where the electric charges of the NN lattice sites overlap. Such an exotic state of matter was recently realized for the first time by our broadband pulse laser excitation that circumvents the Rydberg blockade [36,73].

---

*These authors contributed equally to the work.
†Present address: Department of Physics, Tokyo University of Science, Shinjuku-ku, Tokyo 162-8601, Japan.
‡Present address: Department of Basic Science, The University of Tokyo, Meguro-ku, Tokyo 153-8902, Japan.
§seijisugawa@g.ecc.u-tokyo.ac.jp
‖ohmori@ims.ac.jp

[1] I. M. Georgescu, S. Ashhab, and F. Nori, Quantum simulation, Rev. Mod. Phys. **86,** 153 (2014).

[2] K. Kim, M.-S. Chang, S. Korenblit, R. Islam, E. E. Edwards, J. K. Freericks, G.-D. Lin, L.-M. Duan, and C. Monroe, Quantum simulation of frustrated Ising spins with trapped ions, Nature (London) **465,** 590 (2010).

[3] J. Smith, A. Lee, P. Richerme, B. Neyenhuis, P. W. Hess, P. Hauke, M. Heyl, D. A. Huse, and C. Monroe, Many-body localization in a quantum simulator with programmable random disorder, Nat. Phys. **12,** 907 (2016).

[4] J. G. Bohnet, B. C. Sawyer, J. W. Britton, M. L. Wall, A. M. Rey, M. Foss-Feig, and J. J. Bollinger, Quantum spin dynamics and entanglement generation with hundreds of trapped ions, Science **352,** 1297 (2016).

[5] A. Micheli, G. K. Brennen, and P. Zoller, A toolbox for lattice-spin models with polar molecules, Nat. Phys. **2,** 341 (2006).

[6] B. Yan, S. A. Moses, B. Gadway, J. P. Covey, K. R. A. Hazzard, A. M. Rey, D. S. Jin, and J. Ye, Observation of dipolar spin-exchange interactions with lattice-confined polar molecules, Nature (London) **501,** 521 (2013).

[7] S. Lepoutre, J. Schachenmayer, L. Gabardos, B. Zhu, B. Naylor, E. Maréchal, O. Gorceix, A. M. Rey, L. Vernac, and B. Laburthe-Tolra, Out-of-equilibrium quantum magnetism and thermalization in a spin-3 many-body dipolar lattice system, Nat. Commun. **10,** 1714 (2019).

[8] A. Patscheider, B. Zhu, L. Chomaz, D. Petter, S. Baier, A.-M. Rey, F. Ferlaino, and M. J. Mark, Controlling dipolar exchange interactions in a dense three-dimensional array of large-spin fermions, Phys. Rev. Res. **2,** 023050 (2020).

[9] A. Browaeys and T. Lahaye, Many-body physics with individually controlled Rydberg atoms, Nat. Phys. **16,** 132 (2020).

[10] S. de Léséleuc, V. Lienhard, P. Scholl, D. Barredo, S. Weber, N. Lang, H. P. Büchler, T. Lahaye, and A. Browaeys, Observation of a symmetry-protected topological phase of interacting bosons with Rydberg atoms, Science **365,** 775 (2019).

[11] D. Bluvstein, A. Omran, H. Levine, A. Keesling, G. Semeghini, S. Ebadi, T. T. Wang, A. A. Michailidis, N. Maskara, W. W. Ho, S. Choi, M. Serbyn, M. Greiner, V. Vuletić, and M. D. Lukin, Controlling quantum many-body dynamics in driven Rydberg atom arrays, Science **371,** 1355 (2021).

[12] A. Omran, H. Levine, A. Keesling, G. Semeghini, T. T. Wang, S. Ebadi, H. Bernien, A. S. Zibrov, H. Pichler, S. Choi, J. Cui, M. Rossignolo, P. Rembold, S. Montangero, T. Calarco, M. Endres, M. Greiner, V. Vuletić, and M. D. Lukin, Generation and manipulation of Schrödinger cat states in Rydberg atom arrays, Science **365,** 570 (2019).

[13] N. Takei, C. Sommer, C. Genes, G. Pupillo, H. Goto, K. Koyasu, H. Chiba, M. Weidemüller, and K. Ohmori, Direct observation of ultrafast many-body electron dynamics in an ultracold Rydberg gas, Nat. Commun. **7,** 13449 (2016).

[14] J. Zeiher, R. van Bijnen, P. Schauß, S. Hild, J.-y. Choi, T. Pohl, I. Bloch, and C. Gross, Many-body interferometry of a Rydberg-dressed spin lattice, Nat. Phys. **12,** 1095 (2016).

[15] J. Zeiher, J.-Y. Choi, A. Rubio-Abadal, T. Pohl, R. van Bijnen, I. Bloch, and C. Gross, Coherent Many-Body Spin Dynamics in a Long-Range Interacting Ising Chain, Phys. Rev. X **7,** 041063 (2017).

[16] H. Bernien, S. Schwartz, A. Keesling, H. Levine, A. Omran, H. Pichler, S. Choi, A. S. Zibrov, M. Endres, M. Greiner, V. Vuletić, and M. D. Lukin, Probing many-body dynamics on a 51-atom quantum simulator, Nature (London) **551,** 579 (2017).

[17] P. Schauß, J. Zeiher, T. Fukuhara, S. Hild, M. Cheneau, T. Macrì, T. Pohl, I. Bloch, and C. Gross, Crystallization in Ising quantum magnets, Science **347,** 1455 (2015).

[18] H. Labuhn, D. Barredo, S. Ravets, S. de Léséleuc, T. Macrì, T. Lahaye, and A. Browaeys, Tunable two-dimensional

arrays of single Rydberg atoms for realizing quantum Ising models, Nature (London) **534,** 667 (2016).

[19] V. Lienhard, S. de Léséleuc, D. Barredo, T. Lahaye, A. Browaeys, M. Schuler, L.-P. Henry, and A. M. Läuchli, Observing the Space- and Time-Dependent Growth of Correlations in Dynamically Tuned Synthetic Ising Models with Antiferromagnetic Interactions, Phys. Rev. X **8,** 021070 (2018).

[20] A. Signoles, T. Franz, R. Ferracini Alves, M. Gärttner, S. Whitlock, G. Zürn, and M. Weidemüller, Glassy Dynamics in a Disordered Heisenberg Quantum Spin System, Phys. Rev. X **11,** 011011 (2021).

[21] A. P. Orioli, A. Signoles, H. Wildhagen, G. Günter, J. Berges, S. Whitlock, and M. Weidemüller, Relaxation of an Isolated Dipolar-Interacting Rydberg Quantum Spin System, Phys. Rev. Lett. **120,** 063601 (2018).

[22] E. Guardado-Sanchez, P. T. Brown, D. Mitra, T. Devakul, D. A. Huse, P. Schauß, and W. S. Bakr, Probing the Quench Dynamics of Antiferromagnetic Correlations in a 2D Quantum Ising Spin System, Phys. Rev. X **8,** 021069 (2018).

[23] S. Ebadi, T. T. Wang, H. Levine, A. Keesling, G. Semeghini, A. Omran, D. Bluvstein, R. Samajdar, H. Pichler, W. W. Ho, S. Choi, S. Sachdev, M. Greiner, V. Vuletić, and M. D. Lukin, Quantum phases of matter on a 256-atom programmable quantum simulator, Nature (London) **595,** 227 (2021).

[24] P. Scholl, M. Schuler, H. J. Williams, A. A. Eberharter, D. Barredo, K.-N. Schymik, V. Lienhard, L.-P. Henry, T. C. Lang, T. Lahaye, A. M. Läuchli, and A. Browaeys, Quantum simulation of 2D antiferromagnets with hundreds of Rydberg atoms, Nature (London) **595,** 233 (2021).

[25] S. Geier, N. Thaicharoen, C. Hainaut, T. Franz, A. Salzinger, A. Tebben, D. Grimshandl, G. Zürn, and M. Weidemüller, Floquet Hamiltonian engineering of an isolated many-body spin system, Science **374,** 1149 (2021).

[26] K. Singer, M. Reetz-Lamour, T. Amthor, L. G. Marcassa, and M. Weidemüller, Suppression of Excitation and Spectral Broadening Induced by Interactions in a Cold Gas of Rydberg Atoms, Phys. Rev. Lett. **93,** 163001 (2004).

[27] D. Tong, S. M. Farooqi, J. Stanojevic, S. Krishnan, Y. P. Zhang, R. Côté, E. E. Eyler, and P. L. Gould, Local Blockade of Rydberg Excitation in an Ultracold Gas, Phys. Rev. Lett. **93,** 063001 (2004).

[28] R. Heidemann, U. Raitzsch, V. Bendkowsky, B. Butscher, R. Löw, L. Santos, and T. Pfau, Evidence for Coherent Collective Rydberg Excitation in the Strong Blockade Regime, Phys. Rev. Lett. **99,** 163601 (2007).

[29] A. Gaëtan, Y. Miroshnychenko, T. Wilk, A. Chotia, M. Viteau, D. Comparat, P. Pillet, A. Browaeys, and P. Grangier, Observation of collective excitation of two individual atoms in the Rydberg blockade regime, Nat. Phys. **5,** 115 (2009).

[30] E. Urban, T. A. Johnson, T. Henage, L. Isenhower, D. D. Yavuz, T. G. Walker, and M. Saffman, Observation of Rydberg blockade between two atoms, Nat. Phys. **5,** 110 (2009).

[31] A. Urvoy, F. Ripka, I. Lesanovsky, D. Booth, J. P. Shaffer, T. Pfau, and R. Löw, Strongly Correlated Growth of Rydberg

Aggregates in a Vapor Cell, Phys. Rev. Lett. **114,** 203002 (2015).

[32] H. Schempp, G. Günter, M. Robert-de Saint-Vincent, C. S. Hofmann, D. Breyel, A. Komnik, D. W. Schönleber, M. Gärttner, J. Evers, S. Whitlock, and M. Weidemüller, Full Counting Statistics of Laser Excited Rydberg Aggregates in a One-Dimensional Geometry, Phys. Rev. Lett. **112,** 013002 (2014).

[33] N. Malossi, M. M. Valado, S. Scotto, P. Huillery, P. Pillet, D. Ciampini, E. Arimondo, and O. Morsch, Full Counting Statistics and Phase Diagram of a Dissipative Rydberg Gas, Phys. Rev. Lett. **113,** 023006 (2014).

[34] M. Viteau, P. Huillery, M. G. Bason, N. Malossi, D. Ciampini, O. Morsch, E. Arimondo, D. Comparat, and P. Pillet, Cooperative Excitation and Many-Body Interactions in a Cold Rydberg Gas, Phys. Rev. Lett. **109,** 053002 (2012).

[35] T. Amthor, M. Reetz-Lamour, S. Westermann, J. Denskat, and M. Weidemüller, Mechanical Effect of van der Waals Interactions Observed in Real Time in an Ultracold Rydberg Gas, Phys. Rev. Lett. **98,** 023004 (2007).

[36] M. Mizoguchi, Y. Zhang, M. Kunimi, A. Tanaka, S. Takeda, N. Takei, V. Bharti, K. Koyasu, T. Kishimoto, D. Jaksch, A. Glaetzle, M. Kiffner, G. Masella, G. Pupillo, M. Weidemüller, and K. Ohmori, Ultrafast Creation of Overlapping Rydberg Electrons in an Atomic BEC and Mott-Insulator Lattice, Phys. Rev. Lett. **124,** 253201 (2020).

[37] S. de Léséleuc, D. Barredo, V. Lienhard, A. Browaeys, and T. Lahaye, Analysis of imperfections in the coherent optical excitation of single atoms to Rydberg states, Phys. Rev. A **97,** 053803 (2018).

[38] J. D. Carter and J. D. D. Martin, Coherent manipulation of cold Rydberg atoms near the surface of an atom chip, Phys. Rev. A **88,** 043429 (2013).

[39] T. Baluktsian, B. Huber, R. Löw, and T. Pfau, Evidence for Strong van der Waals Type Rydberg-Rydberg Interaction in a Thermal Vapor, Phys. Rev. Lett. **110,** 123001 (2013).

[40] See Supplemental Material at http://link.aps.org/supplemental/10.1103/PhysRevLett.131.123201 for more details on experimental methods, model fitting, and numerical simulations, which includes Refs. [41–49].

[41] F. Dalfovo, S. Giorgini, L. Pitaevskii, and S. Stringari, Theory of Bose-Einstein condensation in trapped gases, Rev. Mod. Phys. **71,** 463 (1999).

[42] J. F. Sherson, C. Weitenberg, M. Endres, M. Cheneau, I. Bloch, and S. Kuhr, Single-atom-resolved fluorescence imaging of an atomic Mott insulator, Nature (London) **467,** 68 (2010).

[43] G. Alber and P. Zoller, Laser excitation of electronic wave packets in Rydberg atoms, Phys. Rep. **199,** 231 (1991).

[44] K. R. A. Hazzard, B. Gadway, M. Foss-Feig, B. Yan, S. A. Moses, J. P. Covey, N. Y. Yao, M. D. Lukin, J. Ye, D. S. Jin, and A. M. Rey, Many-Body Dynamics of Dipolar Molecules in an Optical Lattice, Phys. Rev. Lett. **113,** 195302 (2014).

[45] I. P. Omelyan, I. M. Mryglod, and R. Folk, Algorithm for Molecular Dynamics Simulations of Spin Liquids, Phys. Rev. Lett. **86,** 898 (2001).

[46] B. DeMarco, C. Lannert, S. Vishveshwara, and T. Wei, Structure and stability of Mott-insulator shells of bosons

trapped in an optical lattice, Phys. Rev. A **71,** 063601 (2005).

[47] A. Browaeys, D. Barredo, and T. Lahaye, Experimental investigations of dipole–dipole interactions between a few Rydberg atoms, J. Phys. B **49,** 152001 (2016).

[48] S. Ravets, H. Labuhn, D. Barredo, T. Lahaye, and A. Browaeys, Measurement of the angular dependence of the dipole-dipole interaction between two individual Rydberg atoms at a Forster resonance, Phys. Rev. A **92,** 020701(R) (2015).

[49] P. Richerme, Z.-X. Gong, A. Lee, C. Senko, J. Smith, M. Foss-Feig, S. Michalakis, A. V. Gorshkov, and C. Monroe, Non-local propagation of correlations in quantum systems with long-range interactions, Nature (London) **511,** 198 (2014).

[50] K. Ohmori, Y. Sato, E. E. Nikitin, and S. A. Rice, High-Precision Molecular Wave-Packet Interferometry with HgAr Dimers, Phys. Rev. Lett. **91,** 243003 (2003).

[51] C. M. Liu, J. Manz, K. Ohmori, C. Sommer, N. Takei, J. C. Tremblay, and Y. Zhang, Attosecond Control of Restoration of Electronic Structure Symmetry, Phys. Rev. Lett. **121,** 173201 (2018).

[52] H. Katsuki, H. Chiba, C. Meier, B. Girard, and K. Ohmori, Actively Tailored Spatiotemporal Images of Quantum Interference on the Picometer and Femtosecond Scales, Phys. Rev. Lett. **102,** 103602 (2009).

[53] M. Kastner, Diverging Equilibration Times in Long-Range Quantum Spin Models, Phys. Rev. Lett. **106,** 130601 (2011).

[54] M. Foss-Feig, K. R. A. Hazzard, J. J. Bollinger, and A. M. Rey, Nonequilibrium dynamics of arbitrary-range Ising models with decoherence: An exact analytic solution, Phys. Rev. A **87,** 042101 (2013).

[55] K. R. A. Hazzard, M. van den Worm, M. Foss-Feig, S. R. Manmana, E. G. Dalla Torre, T. Pfau, M. Kastner, and A. M. Rey, Quantum correlations and entanglement in far-from-equilibrium spin systems, Phys. Rev. A **90,** 063622 (2014).

[56] C. Sommer, G. Pupillo, N. Takei, S. Takeda, A. Tanaka, K. Ohmori, and C. Genes, Time-domain Ramsey interferometry with interacting Rydberg atoms, Phys. Rev. A **94,** 053607 (2016).

[57] R. Mukherjee, T. C. Killian, and K. R. A. Hazzard, Accessing Rydberg-dressed interactions using many-body Ramsey dynamics, Phys. Rev. A **94,** 053422 (2016).

[58] P. Schultzen, T. Franz, S. Geier, A. Salzinger, A. Tebben, C. Hainaut, G. Zürn, M. Weidemüller, and M. Gärttner, Glassy quantum dynamics of disordered Ising spins, Phys. Rev. B **105,** L020201 (2022).

[59] N. Šibalić, J. Pritchard, C. Adams, and K. Weatherill, ARC: An open-source library for calculating properties of alkali Rydberg atoms, Comput. Phys. Commun. **220,** 319 (2017).

[60] Refer to the supplemental material in Ref. [13].

[61] J. Schachenmayer, A. Pikovski, and A. M. Rey, Many-Body Quantum Spin Dynamics with Monte Carlo Trajectories on a Discrete Phase Space, Phys. Rev. X **5,** 011022 (2015).

[62] L. Pucci, A. Roy, and M. Kastner, Simulation of quantum spin dynamics by phase space sampling of Bogoliubov-Born-Green-Kirkwood-Yvon trajectories, Phys. Rev. B **93,** 174302 (2016).

[63] B. Sundar, K. C. Wang, and K. R. A. Hazzard, Analysis of continuous and discrete Wigner approximations for spin dynamics, Phys. Rev. A **99,** 043627 (2019).

[64] M. Kunimi, K. Nagao, S. Goto, and I. Danshita, Performance evaluation of the discrete truncated Wigner approximation for quench dynamics of quantum spin systems with long-range interactions, Phys. Rev. Res. **3,** 013060 (2021).

[65] Y. Chew, T. Tomita, T. P. Mahesh, S. Sugawa, S. de Léséleuc, and K. Ohmori, Ultrafast energy exchange between two single Rydberg atoms on a nanosecond timescale, Nat. Photonics **16,** 724 (2022).

[66] W. Li, C. Ates, and I. Lesanovsky, Nonadiabatic Motional Effects and Dissipative Blockade for Rydberg Atoms Excited from Optical Lattices or Microtraps, Phys. Rev. Lett. **110,** 213005 (2013).

[67] Z. Zhang, M. Yuan, B. Sundar, and K. R. Hazzard, Motional decoherence in ultracold Rydberg atom quantum simulators of spin models, arXiv:2201.08463.

[68] T. L. Nguyen, J. M. Raimond, C. Sayrin, R. Cortiñas, T. Cantat-Moltrecht, F. Assemat, I. Dotsenko, S. Gleyzes, S. Haroche, G. Roux, T. Jolicoeur, and M. Brune, Towards Quantum Simulation with Circular Rydberg Atoms, Phys. Rev. X **8,** 011032 (2018).

[69] C. J. Turner, A. A. Michailidis, D. A. Abanin, M. Serbyn, and Z. Papić, Quantum scarred eigenstates in a Rydberg atom chain: Entanglement, breakdown of thermalization, and stability to perturbations, Phys. Rev. B **98,** 155134 (2018).

[70] C. J. Turner, A. A. Michailidis, D. A. Abanin, M. Serbyn, and Z. Papić, Weak ergodicity breaking from quantum many-body scars, Nat. Phys. **14,** 745 (2018).

[71] D. A. Abanin, E. Altman, I. Bloch, and M. Serbyn, Colloquium: Many-body localization, thermalization, and entanglement, Rev. Mod. Phys. **91,** 021001 (2019).

[72] Y. A. Alaoui, B. Zhu, S. R. Muleady, W. Dubosclard, T. Roscilde, A. M. Rey, B. Laburthe-Tolra, and L. Vernac, Measuring Correlations from the Collective Spin Fluctuations of a Large Ensemble of Lattice-Trapped Dipolar Spin-3 Atoms, Phys. Rev. Lett. **129,** 023401 (2022).

[73] K. Ohmori, Optically engineered quantum states in ultrafast and ultracold systems, Found. Phys. **44,** 813 (2014).